ZnO & Zn_2SnO_4 DYE SENSITIZED SOLAR CELLS

A Senior Honors Thesis

Presented in Partial Fulfillment of the Requirements for graduation with research distinction in the undergraduate colleges of The Ohio State University

by

Elizabeth Toman

The Ohio State University

2007

Project Advisor: Dr. Yiying Wu, Department of Chemistry

Elizabeth Toman, The Ohio State University

Acknowledgments

I would like to thank all who have mentored me in any way throughout my undergrad years. I would like thank Dr. Gustafson for encouragement when life seemed to become overwhelmingly busy. I would also like to thank my advisors, Dr. Pat Woodward, Mrs. Mary Bailey, and Joanna Spanos, for their guidance and mentoring. Specifically, I thank Dr. Woodward for enlightening me about research opportunities such as the research of Dr. Yiying Wu. I would especially like to thank Dr. Wu for not only being a great research advisor but also a great friend. Thank you for understanding my busy schedule and never giving up on me. I started research two years ago without any knowledge about chemistry research, but Dr. Wu helped me transition from the classroom to real life chemistry, preparing me for graduate school and eventually industry. I would also like to thank Dr. Bing Tan, Yanguang Li, and Julia Rabe for helping me throughout lab.

I appreciate my family for helping me finish school. Special thanks to my dad for the late night questions and my mom for emotional support. I also would like to thank my brother for being there whenever I needed him.

Elizabeth Toman, The Ohio State University

Abstract

Due to global warming and a depleting natural gas supply, there is a need to find alternative energy sources. Solar cells have been investigated to combat the energy crisis because they are environmentally safe and use a renewable energy source that is available world-wide, the sun. Dye-sensitized solar cells (DSSC) are attractive because they are cheap and have a long lifetime. Much research has been conducted to create an efficient solar cell. The following research illustrates two different techniques to improve the dye-sensitized solar cell (DSSC). The first technique investigates the use of a nanowire/nanoparticle composite material. DSSCs usually consist of nanocrystals that have a larger surface area to harvest the sunlight. Nanowires have recently been investigated due to their fast electron transport. An investigation was conducted to study the effects of a composite material made from ZnO nanocrystals and nanowires and its effect on the DSSC. Using this ZnO composite, the observed efficiency was greatly improved when compared to pure nanowire. In fact, the efficiency of the infiltrated nanowires when compared to the pure nanowire DSSC increased by a factor of up to 43.6%. The higher efficiency is due to the increased surface area from the nanocrystals as well as maintaining the fast electron transport from the nanowires. The second technique to improve DSSC is the use of a different material: zinc stannate. In previously reported research, the electrode materials have mostly been limited to simple binary oxides. The application of multication oxides in DSSC has been rarely explored. We investigate the application of Zn_2SnO_4 nanoparticles in DSSC. Using Zn_2SnO_4 nanoparticles, an overall light-to-electricity efficiency as high as 3.8% has been achieved. In

comparison with ZnO as its simple component oxide, Zn_2SnO_4 electrode is stable against acidic dye solution. Our results suggest that multication oxides, with the availability of a wide range of compositions and tunable properties, could be promising new electrode materials for DSSCs.

Chapter 1: Introduction

Fossil fuels are being depleted and produce a by-product, carbon dioxide, which is a likely contributor of global warming[1]. There is a need to find alternative forms of energy. Some alternative energy sources such as water or wind are limited to areas with windy environments or flowing rivers. Utilizing energy from the sun allows all parts of the world to use this energy. Solar power from solar cells is not only environmentally safe, but also uses an energy source that will exist for billions of years. The solar cell with the highest efficiency currently, 25%, is a silicon p-n junction solar cell[2]. The problem with these solar cells is its high cost to make. In 1991, Michael Gratzel created a low-cost DSSC with titanium (IV) oxide (a wide band-gap metal oxide) and obtained a solar cell efficiency of 10.4% [3]. Titanium (IV) oxide is widely available and is common in everyday household items, such as sunscreen. Its low production cost, and promising efficiency is ideal for solar cells. Since the breakthrough in 1991, other cheap, other wide band-gap materials such as ZnO[4-5], SnO_2,[6] Nb_2O_5,[7] and In_2O_3.[8] etc. have been widely investigated. Specifically, zinc oxide has received much attention due to its similar band-gap to that of titanium (IV) oxide[9].

The basic mechanism of a DSSC is the conversion of light energy into electrical energy

(Figure 1). In a DSSC, sunlight strikes the dye and excites an electron in a higher molecular orbital. The electron in the higher molecular orbital of the dye is then injected into the conduction band of the semi-conductor (usually titania or zinc oxide). The electron passes from the semiconductor to the electrode and creates a current that drives the work for the system. The electron then routes to the counter electrode and combines with the electrolyte. The electrolyte consists of organic solvent containing an iodide/triiodide redox system. Specifically, the electron from the counter electrode converts triiodide in the electrolyte into iodide. The iodide becomes triiodide again by donating one of its electrons into the empty orbital of the dye, which can in turn be excited by sunlight and injected into the semiconductor. This process occurs quickly and results in no net chemical change[10].

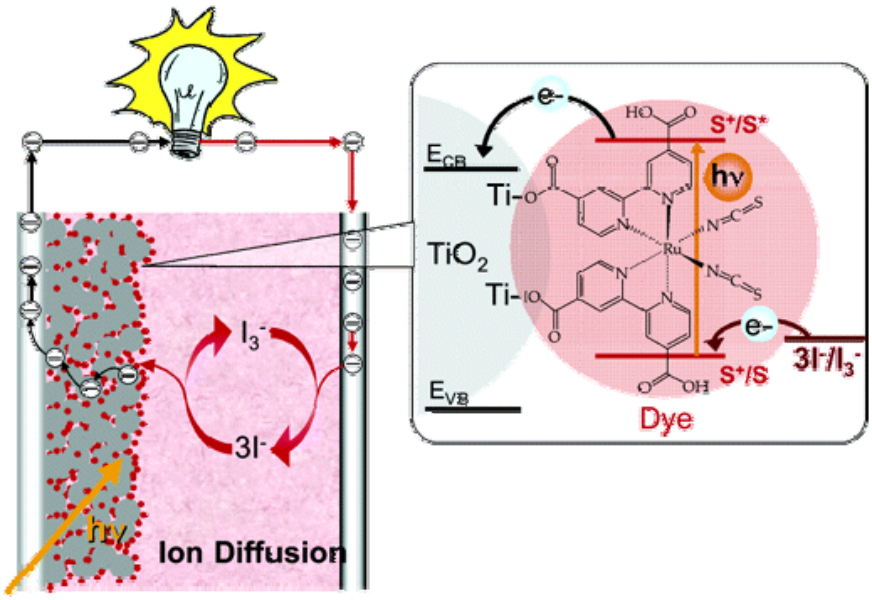

Figure 1 Representation of DSSC (Referenced from Gratzel, *Inorganic Chemistry* 44, 6841 (2005))

Elizabeth Toman, The Ohio State University

Chapter 2: ZnO nanowire/nanoparticle composite

2.1 Background

There are many factors that affect the efficiency of the DSSC. An efficient DSSC requires: (1) a dye with efficient electron injection into the semiconductor, (2) an electrolyte able to penetrate into the porous semiconductor to efficiently reduce oxidized dye molecules, (3) a semiconductor with a large surface area for maximum dye adsorption, and (4) a long diffusion length (fast electron transport) for the injected electrons to be transported.

For a dye to have an efficient electron injection into the semiconductor it has to contain attachment groups, such as carboxylate or phosphate, and the energy of its excited state should match well to the lower bound of the conduction band of the metal oxide. The most important thing to note about the dye is that these dyes are acidic due to the carboxyl groups. The acidic protons can etch ZnO and, therefore, lower the efficiency[11,20].

A large surface area is ideal for DSSC because it maximizes the amount of electrons injected into the semiconductor and, therefore, maximizes photocurrent. For an efficient DSSC the semiconductor must also have a large diffusion length, the distance the electron travels before recombining with the photooxidized dye or electrolyte. Diffusion length (L) can be calculated from the equation: $L= (D_n t_n)^{½}$ where D_n is the electron diffusion coefficient and t_n is the electron lifetime.

The use of nanocrystals and nanowires for DSSC has been widely investigated[3-5,15]. Nanocrystals have a large surface area but a relatively small diffusion coefficient $D_n= 10^{-8}$-$10^{-4} cm^2 s^{-1}$ (titania)[13] and $D_n= 1.7 \times 10^{-4} cm^2 s^{-1}$ (ZnO)[14]. Nanowires have small surface area but larger

diffusion coefficient[5,17] 0.05 -0.5 cm^2 s^{-1}. By combining the two systems, one could potentially obtain a system with relatively high surface area and large diffusion length.

2.2 Experimental

The methodology used was to first make ZnO nanowires and then infiltrate the spaces with ZnO nanocrystals as depicted in Figure 2. The ZnO nanowires were synthesized via a seeded growth mechanism reported previously[5]. These nanowires are optimal because they are vertical nanowires and, therefore, have a larger collection of electrons. The nanowires are also in direct contact with the substrate which maximizes the electron transfer to the electrode. The nanowires were then soaked with a 0.1M zinc nitrate hexahydrate (98%, Aldrich) solution for 30 minutes to allow zinc ion infiltration. The soaked nanowire substrate was then placed in a closed container which contained ammonia vapor overnight to ensure dissolved ammonia in the wet nanowire substrate. The substrate was then placed in an oven and heated to 150 °C for one hour and then heat to 450 ºC for 10 hours.

The obtained product was characterized with X-ray diffraction (XRD, Rigaku), transmission electron microscopy (TEM, Tecnai TF-20), and scanning electron microscope (SEM, Sirion).

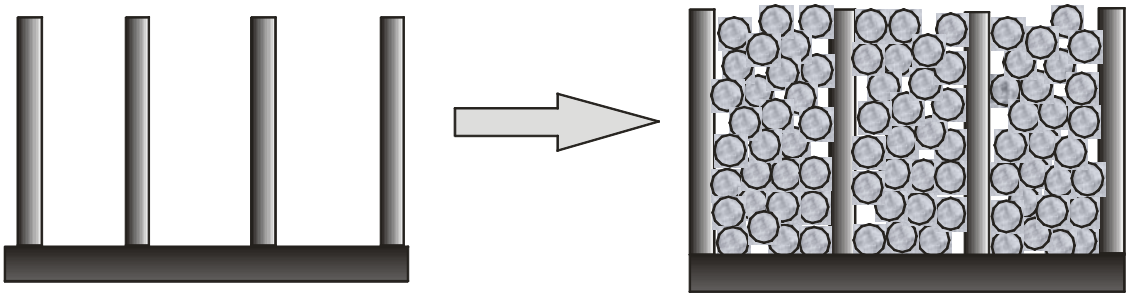

Figure 2 Methodology of ZnO infiltration

2.3 Results and Discussion

The nanowires have been successfully synthesized (Figure 3a) with 4 μm and 10 μm lengths. The ZnO nanowires have also been successfully infiltrated with nanocrystals as can be observed in Figure 3b,c. Figure 3e shows an XRD pattern of the infiltrated nanowires which shows a wurzite structure of the ZnO.

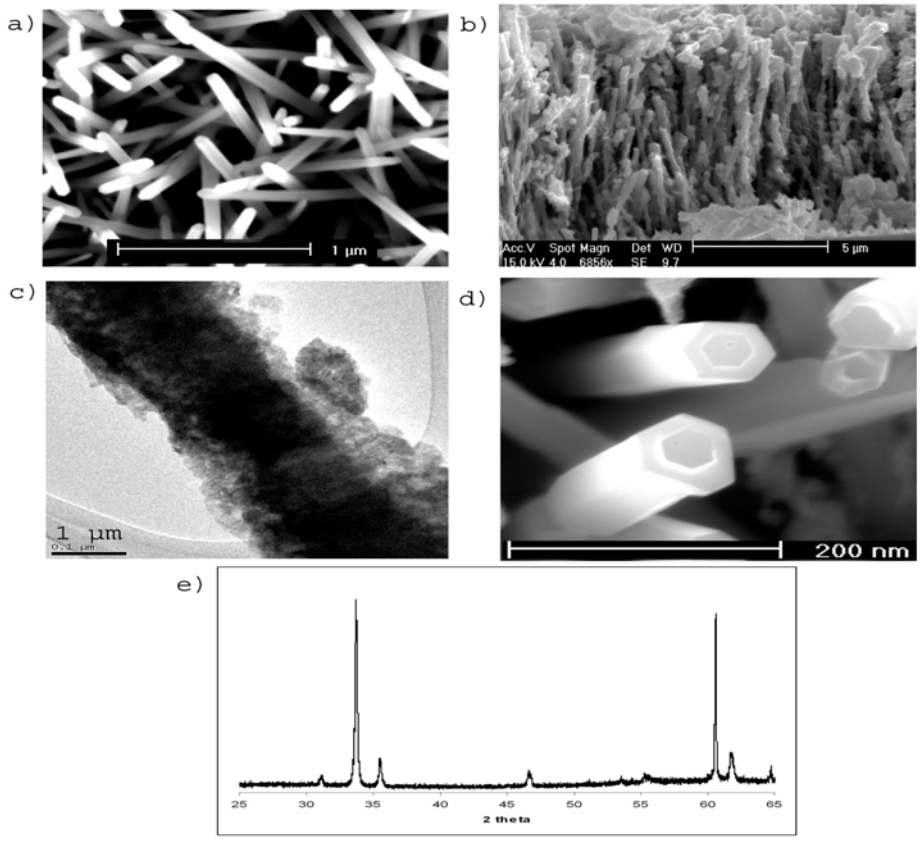

Figure 3 Characterization of the ZnO materials. (a) SEM of bare ZnO nanowires; (b) SEM of infiltrated ZnO nanowires; (c)TEM of infiltrated ZnO nanowires; (d) SEM of etched nanowires due to ammonia; and (e) XRD of the infiltrated nanowires.

The following composite material was tested for solar cell use and was compared to the pure nanowires. The results of the two thicknesses (4 μm and 10 μm length) are shown in table 1

below. For both these samples the nanowires were carefully grown and had uniform diameters. As is observed, the short-circuit current (Jsc) increases with the addition of nanocrystals. This is due to the higher surface area and, therefore, higher electron injection into the semi-conductor. The open-circuit voltage (Voc), also increases. The increased voltage is likely due to the morphology effect. As observed previously[4-5], nanocrystals obtain higher open-circuit voltage when compared to nanowires. The increase in open-circuit voltage for the infiltrated DSSC is a result of the nanocrystals. For both the 4 μm and 10 μm length nanowires the infiltrated nanowires had an increased efficiency. For the 4 μm length the efficiency was increased by 23.4% when compared to the pure nanowire system. Likewise the 10 μm system was improved by 43.6% by infiltration. This increased efficiency is due to an increased surface area.

length	Type of DSSC	Voc (V)	Jsc (mA/cm2)	Fill Factor	Efficiency (%)
4 μm	infiltrated	0.471	1.95	0.289	0.64
	pure wires	0.422	1.55	0.303	0.49
10 μm	infiltrated	0.485	7.52	0.337	1.23
	pure wires	0.435	5.25	0.304	0.694

Table 1. I-V characteristics (under 1 Sun AM 1.5 illumination) for infiltrated ZnO nanowires and pure nanowires for wires of 4 and 10 μm length

It is important to point out that this synthesis poses many problems. In order to grow the nanowires it takes constant changing of solution (every 4 hours for up to a total of 80 hours of reaction time for 20 μm length[5]) for solar cell use. Due to its long synthesis time, this research was not pursued much further. Another problem with this synthesis is the fact that ZnO nanowires can be etched by ammonia (Figure 3d). The system is very sensitive to the amount ammonia vapor and exposure time making it difficult to reproduce. It is also important to note that ZnO is

easily etched away by the acidic dye and therefore does not gain a large efficiency that a titania system would obtain.

2.4 Conclusions

In summary, we have successfully synthesized a ZnO composite. The nanoparticles were tens of nanometers in diameter. Using a composite material consisting of nanoparticles and nanowires a higher efficiency was achieved. Specifically, for the 10 μm length nanowires, the efficiency was increased by 43.6 % by using infiltrated nanoparticles. The improved efficiency can be contributed to an increased surface area and, therefore, higher current. Although the infiltration synthesis is timely, it is important to note the improved efficiency.

Chapter 3: Zn_2SnO_4

3.1 Background

In previously reported research, the electrode materials have mostly been limited to simple binary oxides such as TiO_2, ZnO and SnO_2. In contrast, the application of multication oxides has been rarely explored. To our best knowledge, the only reported ternary oxides are $SrTiO_3$[16] and some doped binary oxides such as La^{3+}- and Zr^{4+}-doped CeO_2.[17]

In comparison with simple binary oxides, multication oxides have more freedom to tune

the materials' chemical and physical properties by altering the compositions. As an example, the ZnO-In_2O_3 ternary compounds have been investigated as new n-type transparent conducting oxide (TCO) materials.[18] By varying the relative Zn/In ratio, the bandgap energy, the work function and the electric resistivity of the ternary oxides can be readily tuned. The ternary oxides also show dramatically reduced acid etching rate in comparison with ZnO. Considering the availability of a wide range of mutication oxides and their tunable properties, it is, therefore, interesting to investigate their applications in DSSC. Potentially, new materials with better performance than anatase TiO_2 could be found. This strategy is similar to the seeking of new TCO materials, which, historically, also started with simple binary oxide materials and then have been gradually expanded to many multi-component oxides.[18]

Our investigation of multi-cation semi-conductors investigates promising application of Zn_2SnO_4 nanoparticles in DSSC. Zn_2SnO_4 is a TCO material with a bandgap of 3.6 eV and electron mobility of 10~15 $cm^2\ V^{-1}s^{-1}$.[19] For the application in DSSC, it is desirable to control the particle size in the range of tens of nanometers to ensure high surface area for dye adsorption.

3.2 Experimental

The controlled synthesis of Zn_2SnO_4 nanoparticles is achieved by decomposing a mixture of zinc- and tin- tert-butylamine complexes under hydrothermal conditions. In a typical synthesis, 0.525 g zinc chloride (98%, Aldrich), 0.675 g tin (IV) chloride pentahydrate (98%, Aldrich) were stirred in 50 ml water-ethylene glycol (1:1 volume ratio) mixed solvent. Then 25 ml 1.3 M tert-butylamine (99%, Acros Organics) aqueous solution was added drop wise to the stirred solution. After stirring for several minutes, the obtained slurry was transferred to a 125 ml autoclave (Parr

Instrument) and heated statically at 175 ºC for overnight. The precipitates from the autoclave were washed several times with water and ethanol to remove the residual amine.

Optimization procedures were also conducted. Such optimization included the temperature of the solution during hydrothermal treatment, surfactant amount, amount of solution present in autoclave, and concentration of the zinc and tin precursors. Specifically, the temperature was varied from 100-250 °C. The temperature did not exceed 250 °C due to instrumental limitations of the autoclave. SDS (sodium dodecyl sulfate) surfactant was added at these temperatures and the effect was observed. The amount of solution was also cut by 50 and 75 %. Finally the concentration of the combined zinc and tin precursors varied from one ninth to nine times the original concentration.

The obtained product was characterized with X-ray diffraction (XRD, Rigaku), transmission electron microscopy (TEM, Tecnai TF-20) and scanning electron microscope (SEM, Sirion).

3.3 Results and discussion

Zn_2SnO_4 was successfully synthesized. The XRD pattern (Figure 4a) confirms that the product is pure Zn_2SnO_4 with the cubic inverse-spinel crystal structure. The average crystal size calculated is around 20 nm. Low magnification TEM (Figure 4b) shows that most obtained nanoparticles have size in the range of 10 to 60 nanometers. This is desirable to provide high surface area for DSSC application. The crystallinity of nanoparticles was further confirmed by the selected-area electron diffraction pattern (Figure 4c) and high resolution TEM (Figure 4d).

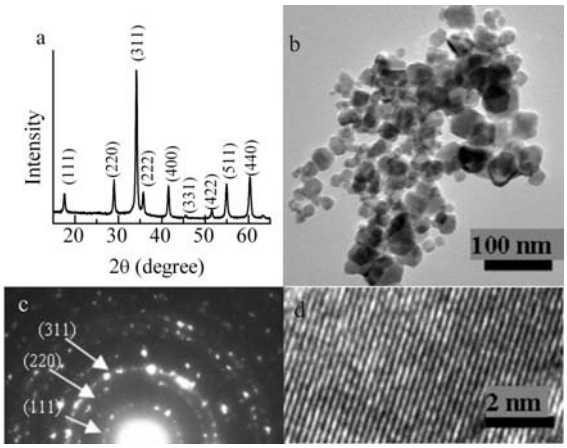

Figure 4. Characterizations of zinc stannate nanoparticles: (a) XRD pattern; (b) Low magnification TEM image; (c) Electron diffraction pattern; and (d) High resolution TEM image (distance between adjacent planes is 2.6 Å, corresponding to d-spacing of (311) planes).

The stability of Zn_2SnO_4 nanoparticles in an acidic dye solution is examined. The solar cell dye used in this investigation is *cis*-bis(isothiocyanato)bis(2,2'-bipyridyl-4,4'-dicarboxylato)-ruthenium(II) bis-tetrabutylammonium (also referred to as N719 or $[RuL_2(NCS)_2]$). Five DSSCs with close thickness of Zn_2SnO_4 nanoparticle film (~ 4.3 μm) were prepared with different sensitization times (Table 2). The dye adsorption (expressed as roughness factor, which is defined as the total surface area per unit substrate area) first increases quickly with the sensitization time in the initial 2 or 6 hours, and then becomes saturated after 1 day. Under 1 Sun AM1.5 illumination, the short-circuit current (J_{sc}) also increases with the sensitization time initially and then becomes saturated. The open-circuit voltage (V_{oc}) and fill factor are stable with various sensitization times. These results suggest that Zn_2SnO_4 is stable against the acidic dye molecules. In reported research, ZnO, which is etched by the acidic dye, has a fast increase in dye adsorption and a large decrease in the short-circuit current due to the formation of aggregates as the case of ZnO.[20] The stability of Zn_2SnO_4 in an acidic dye solution is consistent with the

previous report that Zn_2SnO_4 films can resist the acid etchant.[21]

time	Roughness factor	Jsc (mA/cm2)	Voc (V)	Fill factor	Eff. (%)
2 hr	209	7.6	0.63	0.65	3.1
6 hr	275	8.1	0.63	0.63	3.2
1 day	315	9.1	0.63	0.65	3.7
3 days	338	8.8	0.63	0.64	3.6
7days	309	9	0.63	0.65	3.7

Table 2. Dye adsorption and the I-V characteristics (under 1 Sun AM 1.5 illumination) for cells sensitized with various times

The performance of Zn_2SnO_4 DSSCs with various Zn_2SnO_4 film thicknesses was measured and compared with TiO_2 based DSSCs using P25 nanoparticles (average size: 25 nm). All films made from Zn_2SnO_4 were transparent, while films made from P25 were translucent. For a fair comparison, all films were prepared under similar conditions. The dye sensitization time was 1 day for all cells. Comparisons in dye adsorption, short-circuit current, open-circuit voltage, fill factor, and overall light-to-electricity efficiency are shown in Figure 5.

Figure 5a shows a typical I-V curve for Zn_2SnO_4 cell with a 5.6 μm film thickness. Figure 5b shows the dependence of roughness factor on film thickness. At 10 μm, the roughness factor for a Zn_2SnO_4 film is around 820, which is about twice the amount of dye adsorbed on a P25 film (roughness factor: 440). The high roughness factor for Zn_2SnO_4 film shows that Zn_2SnO_4 can adsorb dye efficiently. The short-circuit current density for Zn_2SnO_4 cells increases initially from 2.8 μm to 4.3 μm, then becomes saturated from 4.3 μm to 7.5 μm, and finally drops down after 7.5 μm (Figure 5c). In comparison, the current density for P25 cells increases with thickness up to 9 μm. This indicates that the electron diffusion length for Zn_2SnO_4 films is shorter than that for

P25 films. For thin films (≤ ~6 μm), the photocurrent for a Zn_2SnO_4 cell is higher than that for a P25 cell of the same film thickness. The open-circuit voltage for a P25 cell is slightly higher than that of a Zn_2SnO_4 cell with the same thickness (Figure 5d), while the fill factor has the opposite relationship (Figure 5e). The overall light-to-electricity efficiency follows the same trend as the photocurrent density for both Zn_2SnO_4 and P25 cells (Figure 5f). For thin films (≤ ~6 μm), the efficiency for a Zn_2SnO_4 cell is higher than that for a P25 cell. The highest energy conversion efficiency that we have achieved from a Zn_2SnO_4 cell is 3.8 % with 5.6 μm film thickness.

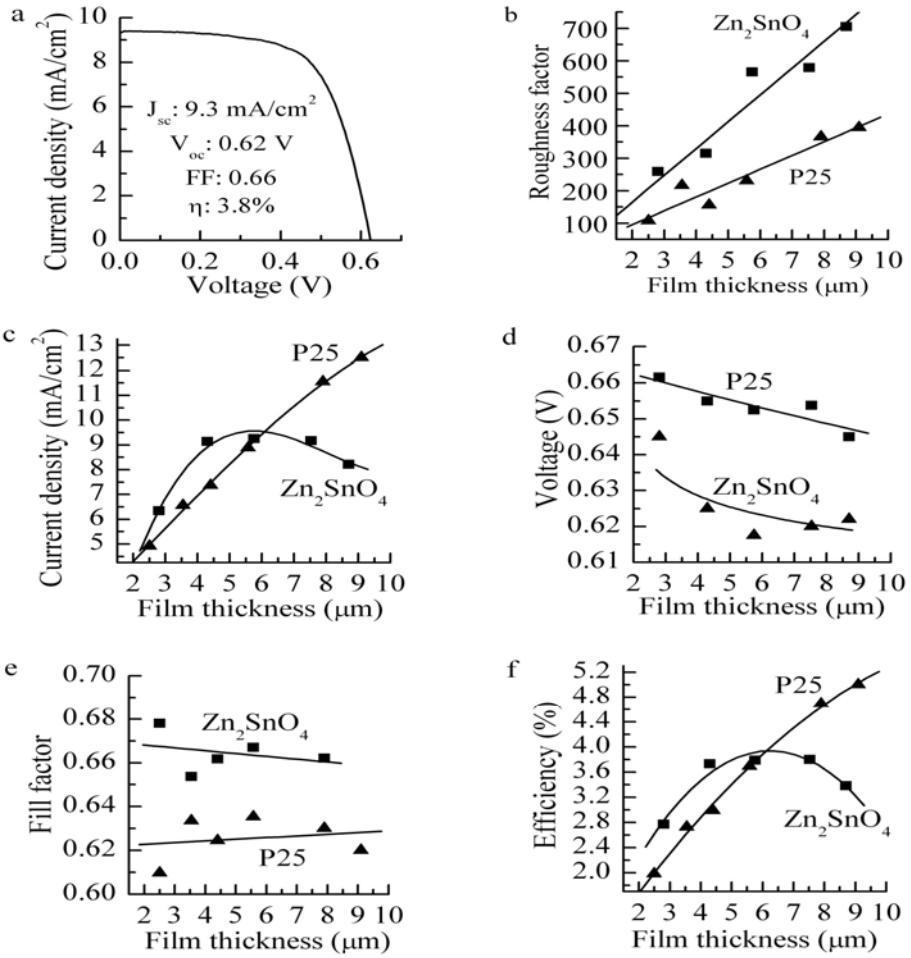

Figure 5. (a). I-V curve of a Zn_2SnO_4 cell with 5.6 μm film thickness; Dependence of cell performance on film thickness: (b). Rough factor; (c). Short-circuit current; (d). Open-circuit voltage; (e). Fill factor; and (f). Overall light-to-electricity efficiency.

It is important to have uniform small particles (~20nm) for solar cells use. To obtain uniformity many parameters were studied for optimization. Such parameters included the temperature heated, surfactant amount, amount of solution, and concentration of zinc- and tin-precursors.

The first optimization procedure was varying the temperature during synthesis. The temperature was varied from 100-250°C. It was observed that when the temperature was increased the particle size increased and became less uniform in size (figure 6 a, b). This fact was observed by SEM pictures as well as XRD analysis. In figure 6 b, one can notice that at 200 °C there is a bimodal distribution of particle size. There are bigger particles with sizes of about 90-150 nm that have a square bipyramidal shape (figure 6c). There also consists of smaller particles with sizes of about 10-20 nm. At 130 °C, there is a decrease in the relative amount of the bigger particles (figure 6 a). The lack of bigger particles is most likely due to decrease of aggregation. As the temperature decreases the zinc stannate particles have fewer chances to aggregate and, therefore, there exists fewer bigger particles. The crystallinity effect of the temperature change has not been investigated currently. As the temperature was increased further, an interesting event took place. At 250 °C, the resultant product was no longer Zn_2SnO_4 but rather formed $ZnSnO_3$ (figure 6 d,e). This is likely due to an increased stability at higher temperature of the $ZnSnO_3$ phase. The stoichiometry suggests that there are excess zinc ions in solution. It is important to note that the XRD displays only the pure phase $ZnSnO_3$ crystalline structure. The lack of ZnO or other zinc compounds suggests that the excess zinc has stayed in solution. Additional tests are needed to confirm this idea.

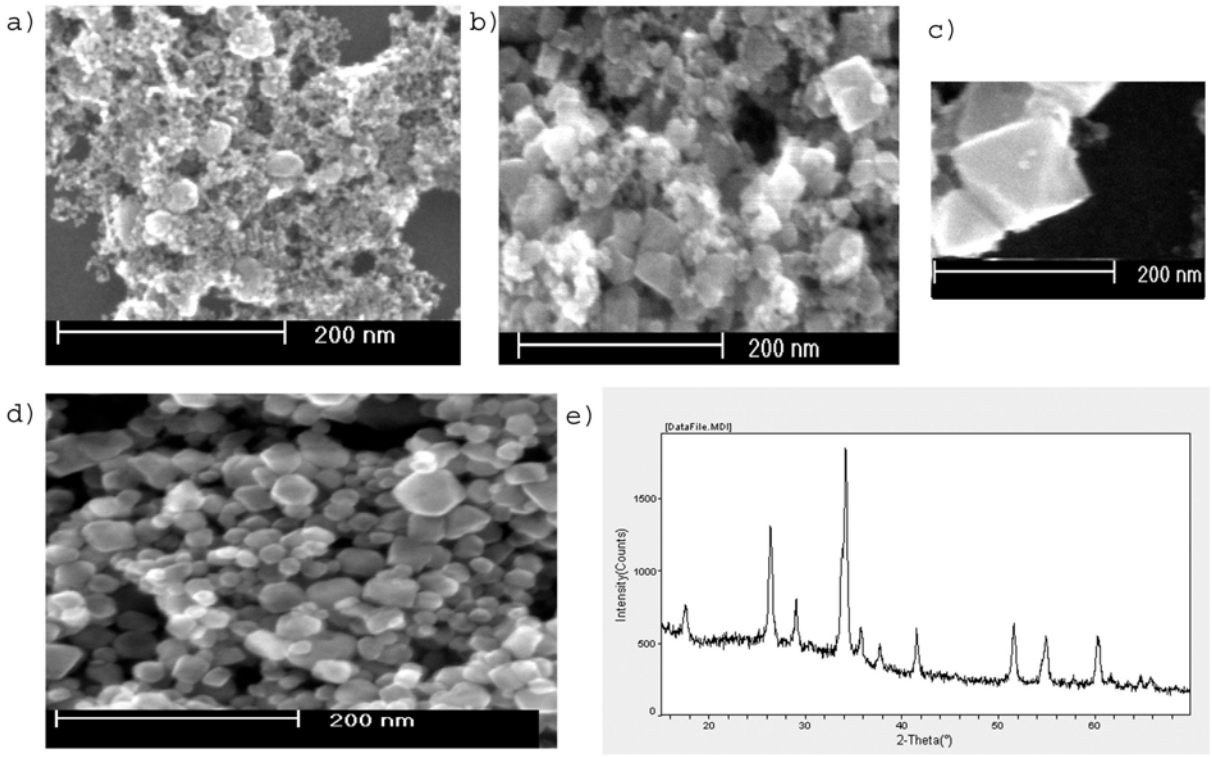

Figure 6. Temperature effects of the zinc stannate synthesis. Effects were observed at: (a) 130°C; (b) 200°C; (c) a large particle at 200 °C; (d) 250 °C formation of $ZnSnO_3$ observed; and (e) XRD of $ZnSnO_3$.

The next parameter varied was the use of surfactant. Various amounts of (0.05-1 g) SDS was added at 200 ˚C. The addition of surfactant decreased the particle size as well as made it more uniform in size (figure 7a, b). When the zinc stannate system that contained no surfactant is compared with 1.0 g of surfactant added there is a decrease in amount of the larger particles. The surfactant interacts electrostatically at the amine-metal complex. As the solution is heated the amine-metal complexes forms zinc stannate. The surfactant surrounded complex hinders the aggregation rate and therefore the larger particles are not observed.

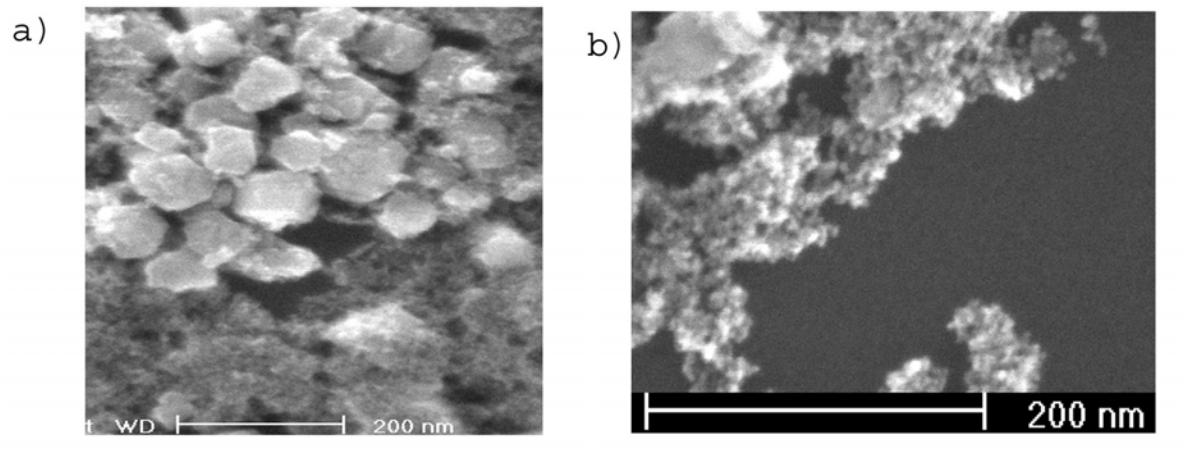

Figure 7. Surfactant effects of the zinc stannate synthesis at 200 °C. SEM characterization containing: (a) no surfactant; and (b) 1.0 g SDS.

The concentration effect on particle size was also investigated (figure 8). The concentration of the zinc and tin precursors varied from one ninth to nine times the original concentration mentioned in the experimental section. The ratio of amine to the precursors remained constant. The results for concentration of the combined zinc and tin precursors were analyzed. Interestingly, as the concentration increased it resulted in a decrease in the amount of larger particles, as well as a decrease in the overall particle size. The effect of concentration on the particle size has been observed previously[22]. As the concentration increases the number of nucleation sites that are saturated increase and therefore form smaller particles. When the concentration is small the number of nuclei is small and therefore the particle size is larger. The limited amount of aggregates could be explained by the increased amount of amine concentration. As the concentration increased the amount of amine added also increased (in order to form the zinc- and tin- tert-butylamine complexes). Once the particles begin to form the amine could have acted as a surfactant limiting the amount of aggregation. Further studies are needed to be

performed to confirm this explanation.

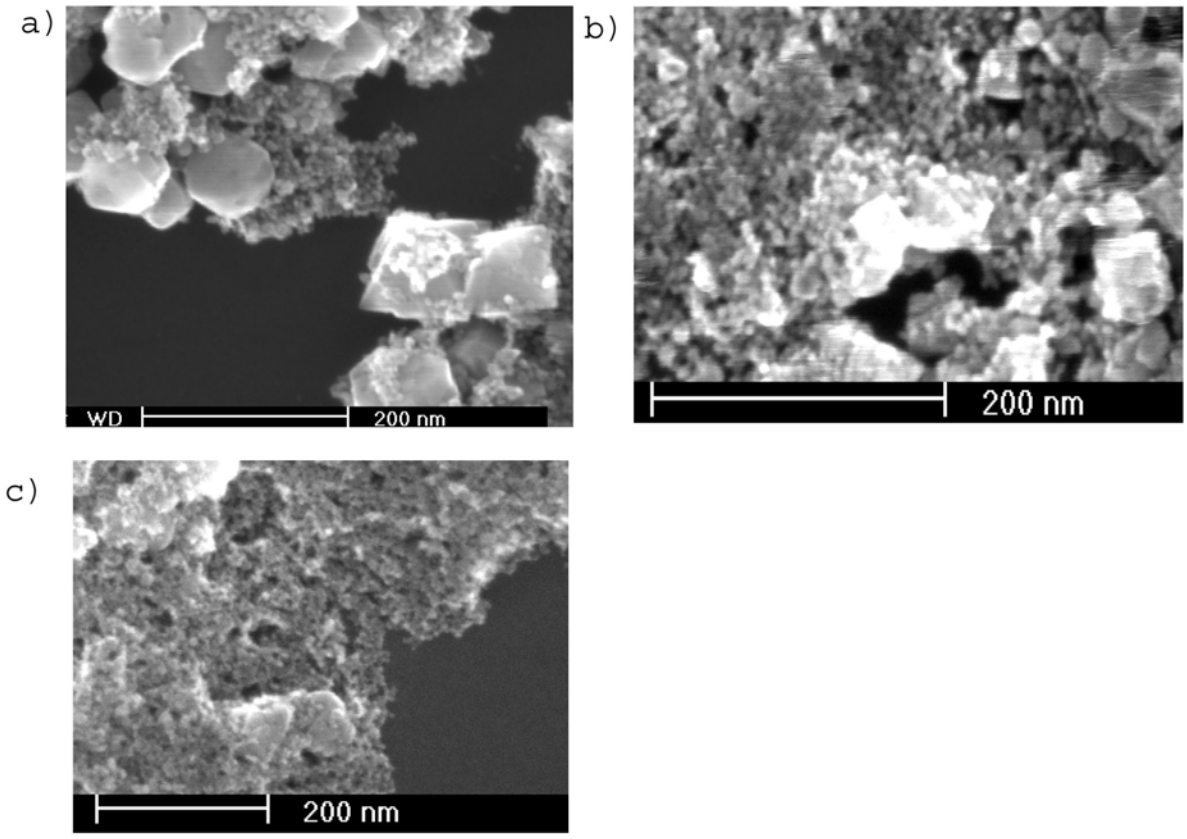

Figure 8. Concentration effects of the zinc stannate synthesis at 200 °C. SEM characterization containing: (a) one third the concentration of the original sample; (b) 3 times the concentration of the original sample; and (c) nine times the concentration of the original sample.

The volume effect was also analyzed. The initial volume was decreased by half and one fourth. Inconsistent results resulted from the experiment (figure 9). As the concentration decreased to half the volume (figure 9b) it resulted in a decrease in particles, as observed in XRD and SEM pictures. When the volume decreased further it resulted in an increase in particle size (figure 9a). This result could be due to non-uniform heating and is currently under investigation.

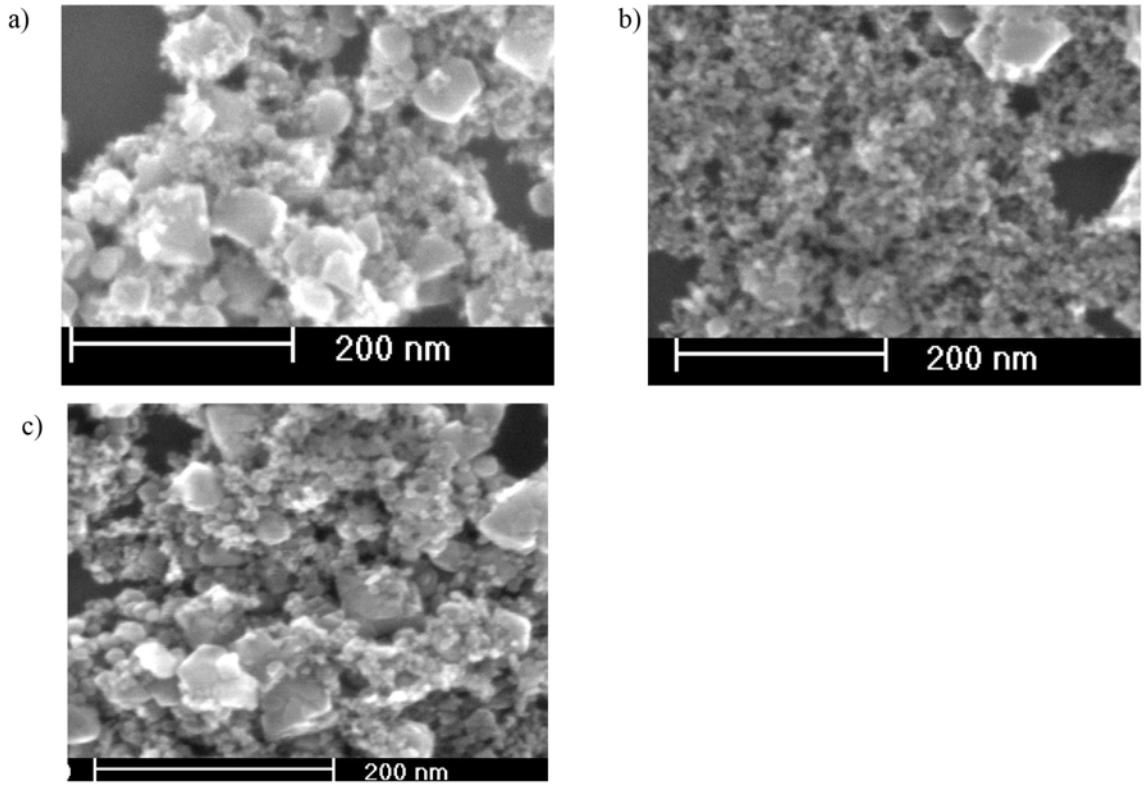

Figure 9. Volume effects of the zinc stannate synthesis at 200 °C. SEM characterization containing: (a) one forth volume of the original sample; (b) one half volume of the original sample; and (c) original volume.

3.4 Conclusions

In summary, we have successfully synthesized Zn_2SnO_4 nanoparticles from a hydrothermal process. In comparison with its simple component oxides (ZnO and SnO_2), Zn_2SnO_4 is stable against acidic dye solution and the cells show higher energy conversion efficiency. We have demonstrated that Zn_2SnO_4 is comparable to TiO_2 for DSSCs in thin films. Because of its large bandgap energy (3.6 eV), Zn_2SnO_4 cells could have better photo-stability against UV light than TiO_2 cells. Currently, the main limitation for Zn_2SnO_4 cells is the short

electron diffusion length as indicated in the trend of J_{sc} with increased film thickness.

Parameters were studied to optimize the synthesis of Zn_2SnO_4. Increasing surfactant, increasing precursor concentration, and decreasing temperature all decreased the particle size. Further studies are needed to investigate the effect of crystallization of these parameters. The effect temperature has on the crystallinity as well as the phase change to $ZnSnO_3$ is under investigation. Future plans to explain the observed optimization results are under way. Such plans include the concentration of the amine and its effect on aggregation rate. Reproducibility of the volume parameter is also to be investigated.

References

1. Hoffert, M. I. *Nature* 1998, 395, 881.
2. Zhao, J.; Wang, A.; Green, M. A. *Prog Photovoltaics* 1999, 7, 471-274.
3. O'Regan, B.; Gratzel , M. *Nature (London, United Kingdom)* 1991, 353, 737-40.
4. Keis, K.; Magnusson, E.; Lindstrom, H.; Lindquist, S.-E.; Hagfeldt, A., Sol. Energ. Mat. Sol. C. 2002, 73, (1), 51-8.
5. (a) Law, M.; Greene, L. E.; Johnson, J. C.; Saykally, R.; Yang, P., Nat. Mater. 2005, 4, (6), 455-9; (b) Martinson, A. B. F.; McGarrah, J. E.; Parpia, M. O. K.; Hupp, J. T., Phys. Chem. Chem. Phys. 2006, 8, (40), 4655-9.
6. Kay, A.; Graetzel, M., Chem. Mater. 2002, 14, (7), 2930-5.
7. a) Guo, P.; Aegerter, M. A., Thin Solid Films 1999, 351, (1,2), 290-4; (b) Sayama, K.; Sugihara, H.; Arakawa, H., Chem. Mater. 1998, 10, (12), 3825-32.
8. Hara, K.; Horiguchi, T.; Kinoshita, T.; Sayama, K.; Sugihara, H.; Arakawa, H., Sol. Energ. Mat. Sol. C. 2000, 64, 115-34.
9. Gratzel, M. *Natutre* 2001, 414, 338-344.
10. Gratzel, M. Journal of Photochemistry and Photobiology A: Chemistry 2004, 164, 3-14.
11. Horiuchi, H.; Katoh, R.; Hara, K.; Yanagida, M.; Murata, S.; Arakawa, H.; Tachiya, M. *Journal of Physical Chemistry B* 2003, 107, 2570-2574.
12. G. Armstrong et al., *Chem. Commun*., **2005**, 2454
13. Kopidakis, N.; Benstein, K. D.; van de Lagemaat, J. & Frank, A.J.; *Journal of Physical Chemistry B.* 2003 (107) 11307-15.
14. Noack, V.; Weller, H.; Eychumuller, A. *Journal of Physical Chemistry B.* 2002, 106, 8514-8523.
15. Goldberger, J.; Sirbuly, D.; Law, M.; Yang, P. *Journal of Physical Chemistry B.* 2005, 109, 9-14.
16. Burnside, S.; Moser, J.-E.; Brooks, K.; Graetzel, M.; Cahen, D., J. Phys. Chem. B 1999, 103, (43), 9328-32.
17. Avelino, C.; Pedro, A.; Hermenegildo, G.; Jean-Yves, C.-C., Nat. mater. 2004, 3, (6), 394-7.
18. Minami, T., MRS Bull. 2000, 25, (8), 38-44.
19. Coutts, T. J.; Young, D. L.; Li, X.; Mulligan, W. P.; Wu, X., J. Vac. Sci. Technol. A 2000, 18, (6), 2646-60.
20. (a) Keis, K.; Lindgren, J.; Lindquist, S.-E.; Hagfeldt, A., Langmuir 2000, 16, (10), 4688 - 94; (b) Law, M.; Greene, L. E.; Radenovic, A.; Kuykendall, T.; Liphardt, J.; Yang, P., J. Phys. Chem. B 2006, 110, (45), 22652-63.
21. Morales-Acevedo, A., Sol. Energy 2006, 80, (6), 675-81.
22. Zhu, H; Zhang, C; Yanshang, Y. Nanotechnology 2005, 16, 3079-3082.